16th World Conference on Earthquake, 16WCEE 2017

Santiago Chile, January 9th to 13th 2017

Paper N° 1699

Registration Code: S-I1461291592

STUDY ON METHOD FOR EVALUATING 3-COMPONENT OF S-WAVES IN SEDIMENTARY LAYERS

H. Kyuke[(1)], Y. Sato[(2)], K. Kobayashi[(3)]

[(1)] Chief Researcher, Research and Development Institute in Takenaka Corporation, kyuuke.hideo@takenaka.co.jp
[(2)] Group Leader, Research and Development Institute in Takenaka Corporation, satou.yoshiyukia@takenaka.co.jp
[(3)] Assistant of Manager, Research and Development Institute in Takenaka Corporation, kobayashi.kikuji@takenaka.co.jp

Abstract

In the study of Kyuke et al. (2010), we proposed a method of evaluating the vertical motion of S-waves, which has been an issue in estimating 3-component waves, by assuming the simultaneous incidence of SV-waves and P-waves in the seismic basement. Using deep borehole records down to the seismic basement, we showed that our proposed method could better predict the observed records than the estimated results by the conventional method, which assuming the oblique incidence of SV-waves in the seismic basement. However, in some period bands of the simulation results, the simulation accuracy is slightly inferior. In this study, in order to improve the simulation accuracy, we focused on the estimation method of the incident wave. Generally, only the deepest sensor's records are used, when the incident wave of the vertical array records was estimated based on the 1-D multiple reflection theory. However, there is a possibility that the estimated incident wave is distorted, because the incident wave can fully predict the record of the deepest sensor, although the assumed ground model might include an error. Thus, in this study, we introduced a new technique to the method of Kyuke et al. (2010). The new technique estimates the incident wave in the seismic basement using all of the array records. Further, this method was extended to the SH incident wave. Then, we simulated the 3-component records of a deep borehole down to the seismic basement. We confirm that these results are more consistent with the observed records than the conventional approaches.

Keywords: Evaluating S-waves motions, P-wave, SV-wave, SH-wave, Simultaneous Incidence

1. Introduction

In estimating 3-component waves in sedimentary layers, the method of estimating the vertical motion of the S-waves has been an issue for many years. For the vertical component of the S-waves in shallow ground, there are several studies that show that the vertical component is rich in P-waves converted from SV incident waves in the seismic basement[1] [2]. Hence, an evaluation method assuming oblique incidence of SV-waves in the seismic basement is often used. However, there is a study that shows the possibility that the vertical component of the statistical Green's function is underestimated by using the ground amplification based on the assumption of the oblique incidence of the SV-wave[3]. Thus, we cannot say that this assumption it is sufficient to explain the vertical component. Based on the above, in the study of Kyuke et al. (2010) [4], we studied the incident wave in the seismic basement that forms the vertical component of the S-waves. We confirmed that the subsequent P-wave in the seismic basement continues with large amplitude until after the arrival of the S-wave. Further, we showed that the simultaneous incidence of SV-waves and P-waves in the seismic basement is required for evaluating of the vertical component of the S-waves. We proposed a method of evaluating vertical and horizontal radial motion of S-waves assuming the simultaneous incidence of SV-waves and P-waves in the seismic basement. Using this method, we simulated the vertical and horizontal radial components of the deep borehole records down to the seismic basement. This showed better agreement with the observed records than the result estimated by assuming a conventional SV-wave oblique incidence. However, in some period band of the simulated results, the simulation accuracy is slightly inferior.

In this study, in order to improve the simulation accuracy, we focused on the estimation method of the incident wave. Generally, only the deepest sensor's records are used when the incident wave of the vertical array records is estimated based on 1-D multiple reflection theory. However, there is a possibility that the estimated incident wave is distorted, because it can fully predict the record of the deepest sensor, although the assumed ground model might include an error. Thus, in this study we introduced a new technique to the method of Kyuke et al.(2010). This involves estimating the incident wave of the seismic basement using all of the array records. Further, this method was extended to the SH incident wave in order to apply 3- component motions.

By using the proposed method, we simulated the 3-component vertical array records down to the seismic basement. Then, we compared the results of our method with the results of assuming oblique incidence of SV-wave, to verify the validity of this method.

2. Analysis Method

An overview of the evaluation method of the vertical and radial components of an S-wave in sedimentary layers, considering the simultaneous incidence of the SV-wave and P-wave (Kyuke et al. (2010)), is as follows:

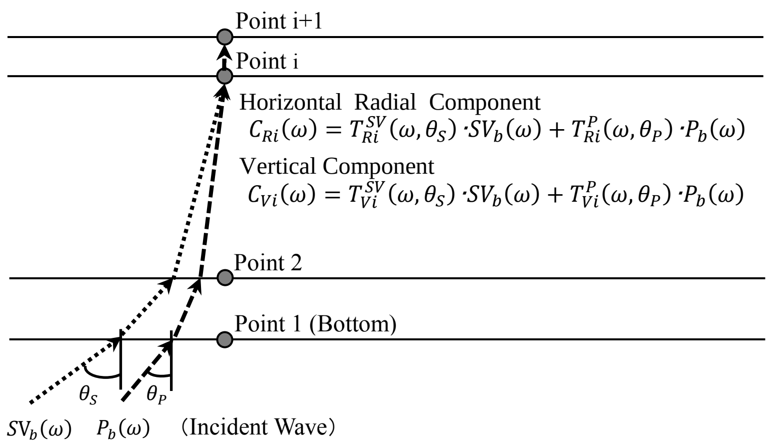

Fig. 1 - Evaluation method of the vertical and radial components of an S-wave in sedimentary layers.

Assume that the incident of the SV-wave and P-wave in the bottom layer of the horizontal multi-layer structure is as shown in Fig. 1. Here, if we set the incident wave spectrum as $SV_b(\omega)$ and $P_b(\omega)$, the Fourier transform of the horizontal radial and vertical components motion at Point i, which are generated from multiple reflections, is written as equation (1):

$$\begin{Bmatrix} C_{Ri}(\omega) \\ C_{Vi}(\omega) \end{Bmatrix} = \begin{Bmatrix} T^{SV}_{Ri}(\omega, \theta_S) \\ T^{SV}_{Vi}(\omega, \theta_S) \end{Bmatrix} SV_b(\omega) + \begin{Bmatrix} T^{P}_{Ri}(\omega, \theta_P) \\ T^{P}_{Vi}(\omega, \theta_P) \end{Bmatrix} P_b(\omega) \tag{1}$$

where $C_{Ri}(\omega)$ and $C_{Vi}(\omega)$ are the theoretical values of the horizontal radial and vertical components motion at Point i, respectively; $T^{SV}_{Ri}(\omega, \theta_S)$ and $T^{SV}_{Vi}(\omega, \theta_S)$ are the transfer functions for the horizontal radial and vertical components, respectively, at Point i resulting from SV incidence waves; $T^{P}_{Ri}(\omega, \theta_P)$ and $T^{P}_{Vi}(\omega, \theta_P)$ are transfer functions for the horizontal radial and vertical components, respectively, at Point i resulting from P incidence waves; ω is the angular frequency; and θ_S and θ_P are the incident angles of the SV-waves and P-waves, respectively.

Then, incident wave spectrums $SV_b(\omega)$ and $P_b(\omega)$ are estimated based on the observed value at point 1 of the horizontal radial component $O_{R1}(\omega)$ and the vertical component $O_{V1}(\omega)$, as shown in equation (2). The incident wave spectrums have been used to simulate the motion at any point by substitution into equation (1).

$$\begin{Bmatrix} SV_b(\omega) \\ P_b(\omega) \end{Bmatrix} = \begin{bmatrix} T^{SV}_{R1}(\omega,\theta_S) & T^{P}_{R1}(\omega,\theta_P) \\ T^{SV}_{V1}(\omega,\theta_S) & T^{P}_{V1}(\omega,\theta_P) \end{bmatrix}^{-1} \begin{Bmatrix} O_{R1}(\omega) \\ O_{V1}(\omega) \end{Bmatrix} \tag{2}$$

However, as can be seen from equation (2), $SV_b(\omega)$ and $P_b(\omega)$ are affected by the accuracy of the theoretical transfer functions calculated from the ground model. That is, these incident waves are estimated in order to explain only the bottom observation records, and thus it is possible that these incident waves will not successfully explain other array records.

In order to increase the estimation accuracy of the incident waves, we estimate the incident waves with all the vertical array records using the linear least squares method. Further, equation (2), although described with respect to SV and P incident waves only, is also simultaneously estimated for the SH incident wave.

The procedure of estimating the incident waves is shown below. First, applying equation (1) for each observation point of the vertical array, and summarize in vector form in equation (3).

$$\begin{Bmatrix} C_{Rn}(\omega) \\ \vdots \\ C_{R1}(\omega) \\ C_{Vn}(\omega) \\ \vdots \\ C_{V1}(\omega) \end{Bmatrix} = \begin{Bmatrix} T^{SV}_{Rn}(\omega,\theta_S) \\ \vdots \\ T^{SV}_{R1}(\omega,\theta_S) \\ T^{SV}_{Vn}(\omega,\theta_S) \\ \vdots \\ T^{SV}_{V1}(\omega,\theta_S) \end{Bmatrix} SV_b(\omega) + \begin{Bmatrix} T^{P}_{Rn}(\omega,\theta_P) \\ \vdots \\ T^{P}_{R1}(\omega,\theta_P) \\ T^{P}_{Vn}(\omega,\theta_P) \\ \vdots \\ T^{P}_{V1}(\omega,\theta_P) \end{Bmatrix} P_b(\omega) \tag{3}$$

Further, equation (3) is expanded into equation (4), taking into account the horizontal transverse component:

$$\begin{Bmatrix} C_{Rn}(\omega) \\ \vdots \\ C_{R1}(\omega) \\ C_{Vn}(\omega) \\ \vdots \\ C_{V1}(\omega) \\ C_{Tn}(\omega) \\ \vdots \\ C_{T1}(\omega) \end{Bmatrix} = \begin{Bmatrix} T^{SV}_{Rn}(\omega,\theta_S) \\ \vdots \\ T^{SV}_{R1}(\omega,\theta_S) \\ T^{SV}_{Vn}(\omega,\theta_S) \\ \vdots \\ T^{SV}_{V1}(\omega,\theta_S) \\ 0 \\ \vdots \\ 0 \end{Bmatrix} SV_b(\omega) + \begin{Bmatrix} T^{P}_{Rn}(\omega,\theta_P) \\ \vdots \\ T^{P}_{R1}(\omega,\theta_P) \\ T^{P}_{Vn}(\omega,\theta_P) \\ \vdots \\ T^{P}_{V1}(\omega,\theta_P) \\ 0 \\ \vdots \\ 0 \end{Bmatrix} P_b(\omega) + \begin{Bmatrix} 0 \\ \vdots \\ 0 \\ 0 \\ \vdots \\ 0 \\ T^{SH}_{Tn}(\omega,\theta_S) \\ \vdots \\ T^{SH}_{T1}(\omega,\theta_S) \end{Bmatrix} SH_b(\omega) \tag{4}$$

where $SH_b(\omega)$ is the incident wave spectrum of the SH wave, $T^{SH}_{Ti}(\omega,\theta_S)$ is the transfer function of each observation point for the SH incident wave, and $C_{Ti}(\omega)$ is the theoretical value of the horizontal transverse component at each observation point.

Summarizing equation (4) in a matrix format yields equation (5):

$$\left\{\overline{C}(\omega)\right\} = \left[\left\{\overline{T^{SV}}(\omega,\theta_S)\right\} \left\{\overline{T^{P}}(\omega,\theta_P)\right\} \left\{\overline{T^{SH}}(\omega,\theta_S)\right\}\right] \begin{Bmatrix} SV_b(\omega) \\ P_b(\omega) \\ SH_b(\omega) \end{Bmatrix} \tag{5}$$

where $\left\{\overline{C}(\omega)\right\}$ is a column vector of the Fourier transforms of the horizontal and vertical motions, which are calculated at each observation point; and $\left\{\overline{T^{SV}}(\omega,\theta_S)\right\}$, $\left\{\overline{T^{P}}(\omega,\theta_P)\right\}$ and $\left\{\overline{T^{SH}}(\omega,\theta_S)\right\}$ are the column vectors of the transfer functions for each SV, P, and SH incident wave, respectively.

Then, we convert the observed waveforms to Fourier transform, and summarize them as $\left\{\overline{O}(\omega)\right\}$ in the same manner as in the column vector format $\left\{\overline{C}(\omega)\right\}$, and estimate $SV_b(\omega)$, $P_b(\omega)$ and $SH_b(\omega)$ to minimize equation (6). These are the incident spectrums to be used in the simulation.

$$E(\omega) = \sum\left(\left\{\overline{O}(\omega)\right\} - \left\{\overline{C}(\omega)\right\}\right)^2 \tag{6}$$

3. Simulation of the observed wave

3.1 Earthquake records and ground model

We simulated the 3-component records from the Iwaki observation point (IWK) in Hukushima prefecture, which has six vertical array observation points at various depths, down to the seismic basement. These records are part of the data of the vertical seismic array network over Fukushima and the Kanto region, published by twelve Japanese power companies[5]. The analysis duration was twenty seconds, beginning one second prior to the arrival of the S-wave. The ground model of Iwaki is shown in Fig. 2. The velocity structure was set by PS logging, and Q-values were estimated by inverse analysis of the transfer function of the vertical array records. In case of estimating of the Q value, Qs was determined by the analysis of SH wave oblique incidence using the S-wave horizontal transverse component, and Qp by analysis of the P-wave oblique incidence using the P-wave vertical component. Fig. 3 shows the epicenter location of the earthquake used in this study. The earthquake information is indicated in Table 1. The angles of incidence shown were assumed on the basis of the particle motion of the initial motions of the P-waves, and the initial motion of the S-waves in the seismic basement (GL-330 m). These angles of incidence were used in the simulation described below.

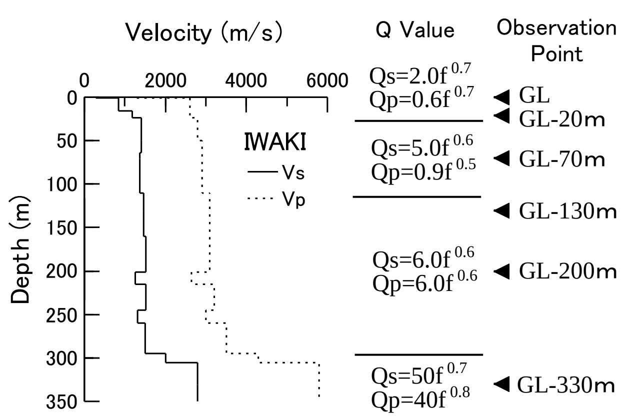

Fig. 2 - Underground model and seismometer position at Iwaki observation point.

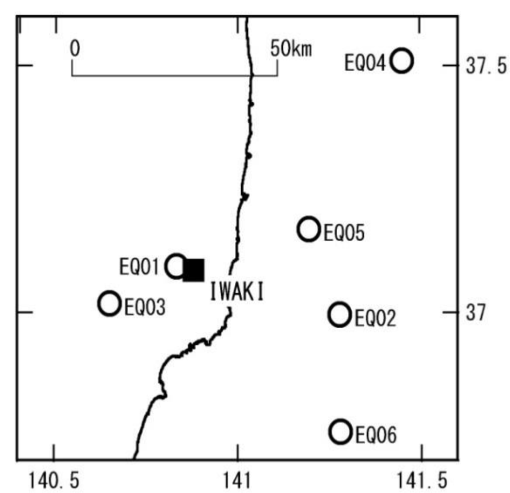

Fig. 3 - Map of epicenter used for this study.

Table 1 - IWAKI Earthquake Information

	Date (mm/dd/yy)	Origin Time	Mj*	Depth (km)	Epicentral distance (km)	Assumed incident angle θ_P, θ_S (°)
EQ01	4/17/2011	23:46	4.5	6.6	4	30, 30
EQ02	4/18/2011	00:47	4.8	29.4	37	30, 30
EQ03	4/19/2011	15:53	4.6	6.5	22	30, 30
EQ04	4/22/2011	01:11	5.6	48.2	69	25, 25
EQ05	4/23/2011	00:25	5.4	21.4	29	25, 25
EQ06	4/30/2011	14:06	5.3	36.9	51	30, 30

* Mj is the local magnitude defined and calculated by Japan Meteorological Agency(JMA).

3.2 Simulation result

We examine the simulation results of the vertical, horizontal radial, and horizontal transverse components calculated from the proposed method. As an example, the comparison between the simulation results and the observation records of EQ06 are shown in Fig. 4 ~ Fig. 6. Fig. 4 shows the simulated waveform, Fig. 5 the transfer function of each observation point for the bottom layer (GL-330 m), and Fig. 6 the pseudo-velocity response spectrum (h = 0.05). For comparison, Fig. 5 and Fig. 6 show the simulation results of conventional oblique SV wave incidence, which is often used in the estimation of the vertical and horizontal radial components. Note that the results of the oblique incidence of the SV-wave are also simulated based on the incident wave of all records of the array. The simulation results assuming the simultaneous incidence of the SV-wave and P-wave are consistent with the observed records in terms of waveforms, transfer functions, and response spectrums of each component.

Then, we compare the simulation results of the proposed method with the results assuming the oblique incidence of the SV-wave. Focusing on vertical component, the transfer functions by SV-wave incidence in Fig. 5(a) show a smoother and simpler shape than those of the observed transfer functions, thus they do not express the fine spectral shape of the observed records. On the other hand, the transfer functions by our proposed method are well-matched to the fine shape of the spectrums. In Fig. 6(a), the response spectrums assuming SV-wave incidence are more greatly underestimated than the observed response spectrums in short periods less than 0.3 s. On the other hand, the response spectrums by our proposed method are well-matched to the observed response spectrums. Focusing on horizontal radial component, the transfer functions in Fig. 5(b) and response spectrums in Fig. 6(b) show that both of the results by our proposed method and those assuming SV-wave incidence are consistent with the observed records, to the same degree.

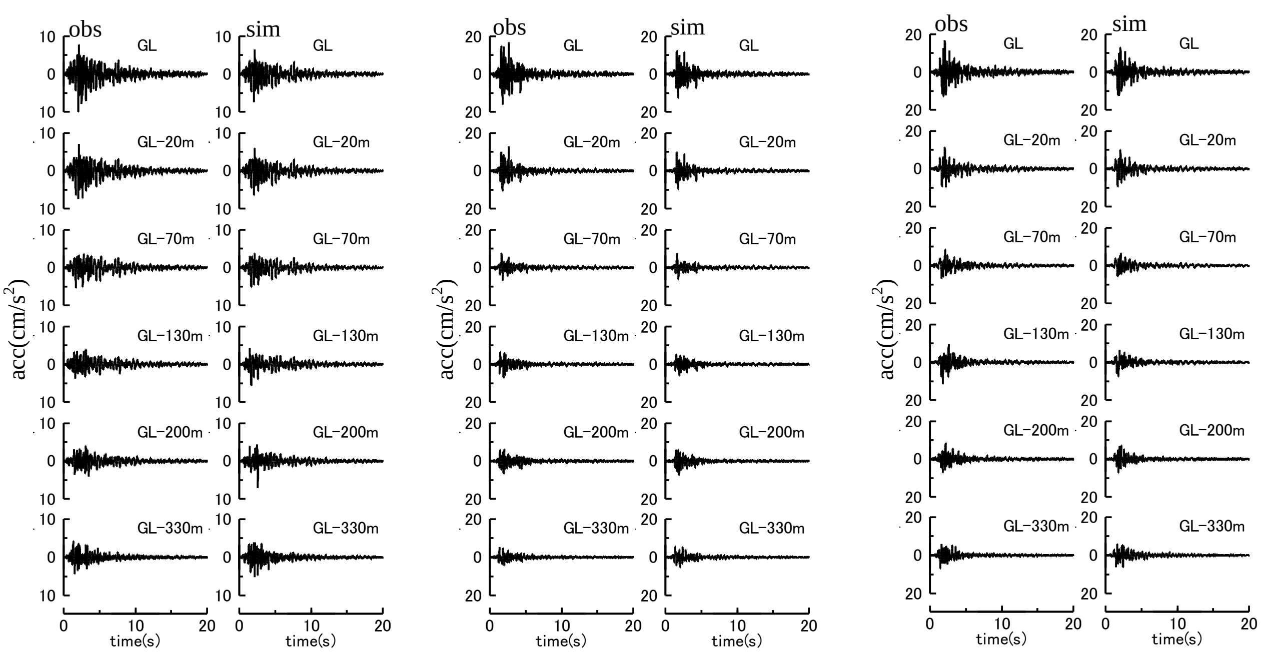

(a) vertical component (b) horizontal radial component (c) horizontal transverse component

Fig. 4 - Comparison of the waveforms by simulation and observation (EQ06).

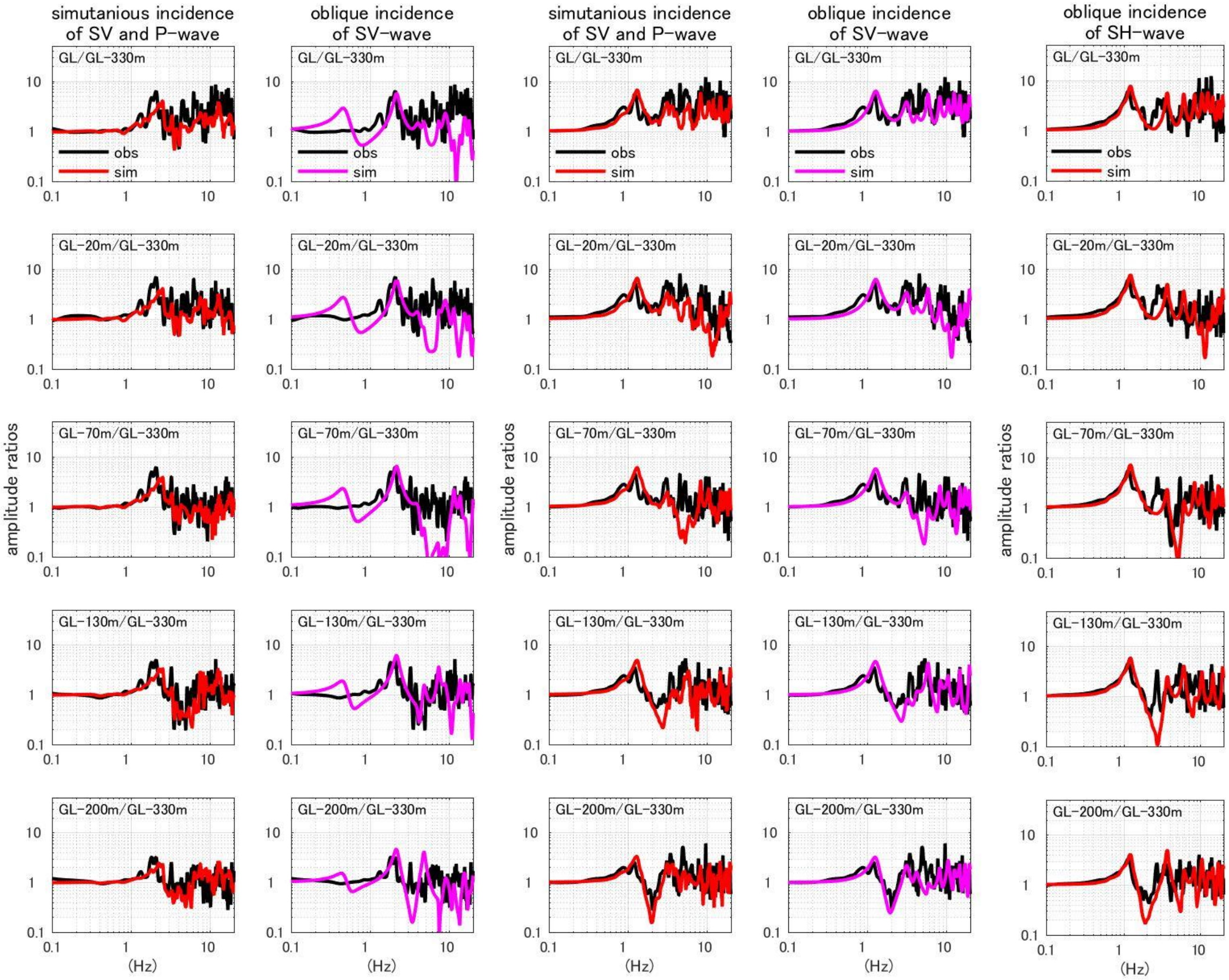

(a) vertical component (b) horizontal radial component (c) horizontal transverse component

Fig. 5 - Comparison of the transfer functions by simulation and observation (EQ06).

In order to evaluate other earthquake records, we compare the simulation results with the observed records of all six earthquakes used in the study. Fig. 7 shows the response spectra ratios of the simulations and the observed records, where the black lines indicate the mean value. The vertical component in Fig. 7(a) shows that the results by SV-wave incidence are underestimated in short periods of less than 0.3 s, e.g., in the valley around the period 0.2 s at GL-20m, is 0.2 times greater than the observed value. Conversely, the results of the SV and P-wave simultaneous incidence in Fig. 7 (a) shows the average value approximates one at all depths, which is a good agreement with the observed records. On the other hand, focusing on the horizontal radial component of Fig. 7 (b), the results of both our proposed method and that by assuming SV-wave incidence are consistent with the observed records to the same degree. This is also able to better explain the observations recorded for the horizontal transverse component of Fig. 7 (c). This analysis confirms that for the vertical component of S-wave, our proposed method is able to more accurately predict the observed records than the oblique incidence of the SV-wave, and for the radial component of the S-waves, our proposed method and the method of oblique incidence of the SV-wave accurately predict the observation records to the same degree.

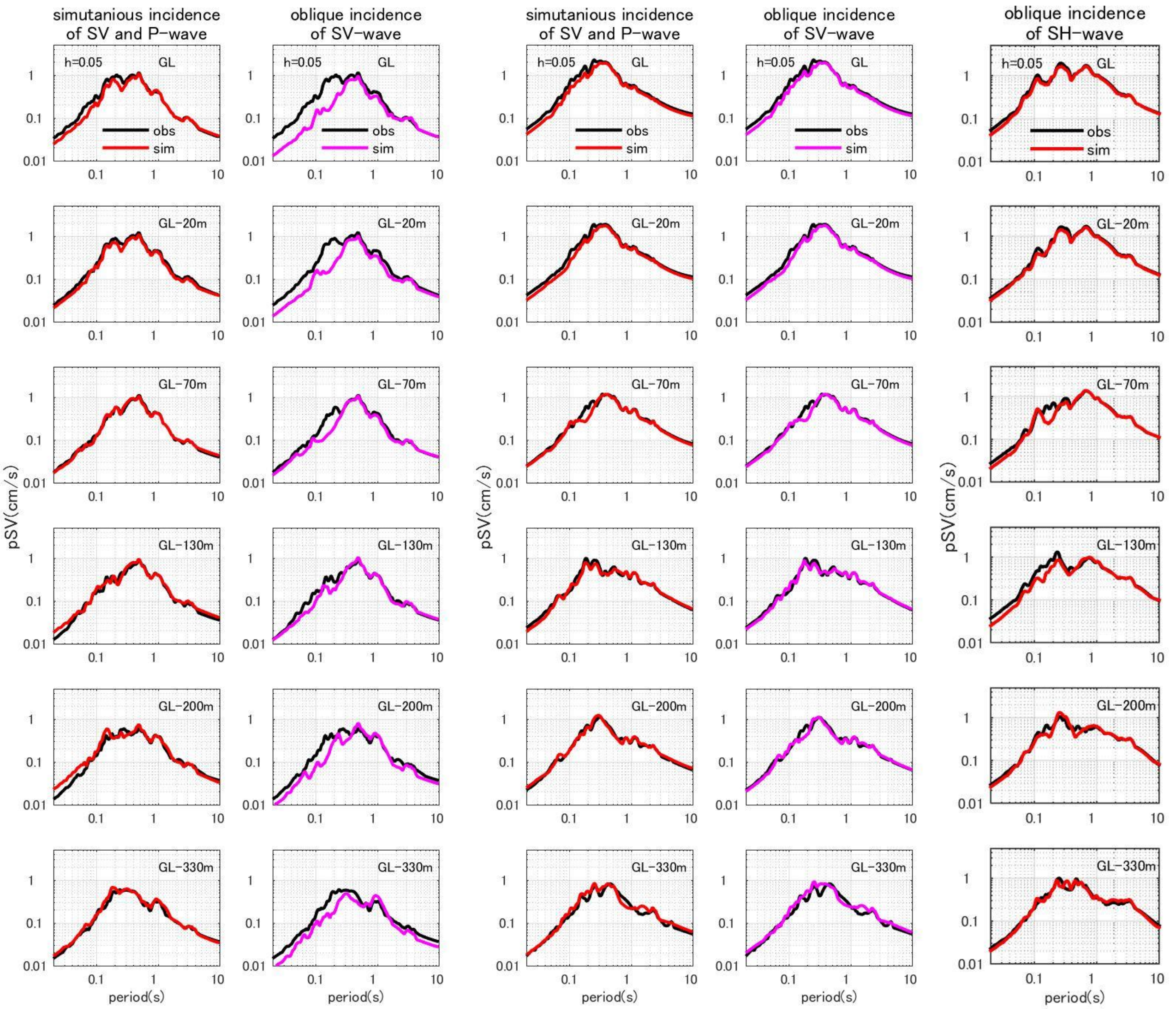

(a) vertical component (b) horizontal radial component (c) horizontal transverse component

Fig. 6 - Comparison of the response spectrums by simulation and observation (EQ06).

In order to confirm the effect of the new method that estimates incident waves using all the records of vertical array, we compare the simulation results before and after the improvements. As an example, the simulation results of the vertical component are shown in Fig. 8. Each line indicates the average value of the response spectrum ratios of the simulated waves to the observed records of six earthquake records, where the black and red lines show the before and after improvement values, respectively. As previously mentioned, the results show that for GL-330 m, the simulation result and observed value before improvement are in agreement because the incident wave is estimated from the observed value of this point. At a period of approximately 0.4 s, there are big residuals between the simulation results by the before-improvement method and the observations records. Conversely, there is no divergence between the simulation results by the after-improvement method and the observations records, the correlation is greatly improved. Further, although not shown, for the horizontal radial and transverse components, residuals between the simulated results by the after-improvement method and observed records were greatly reduced.

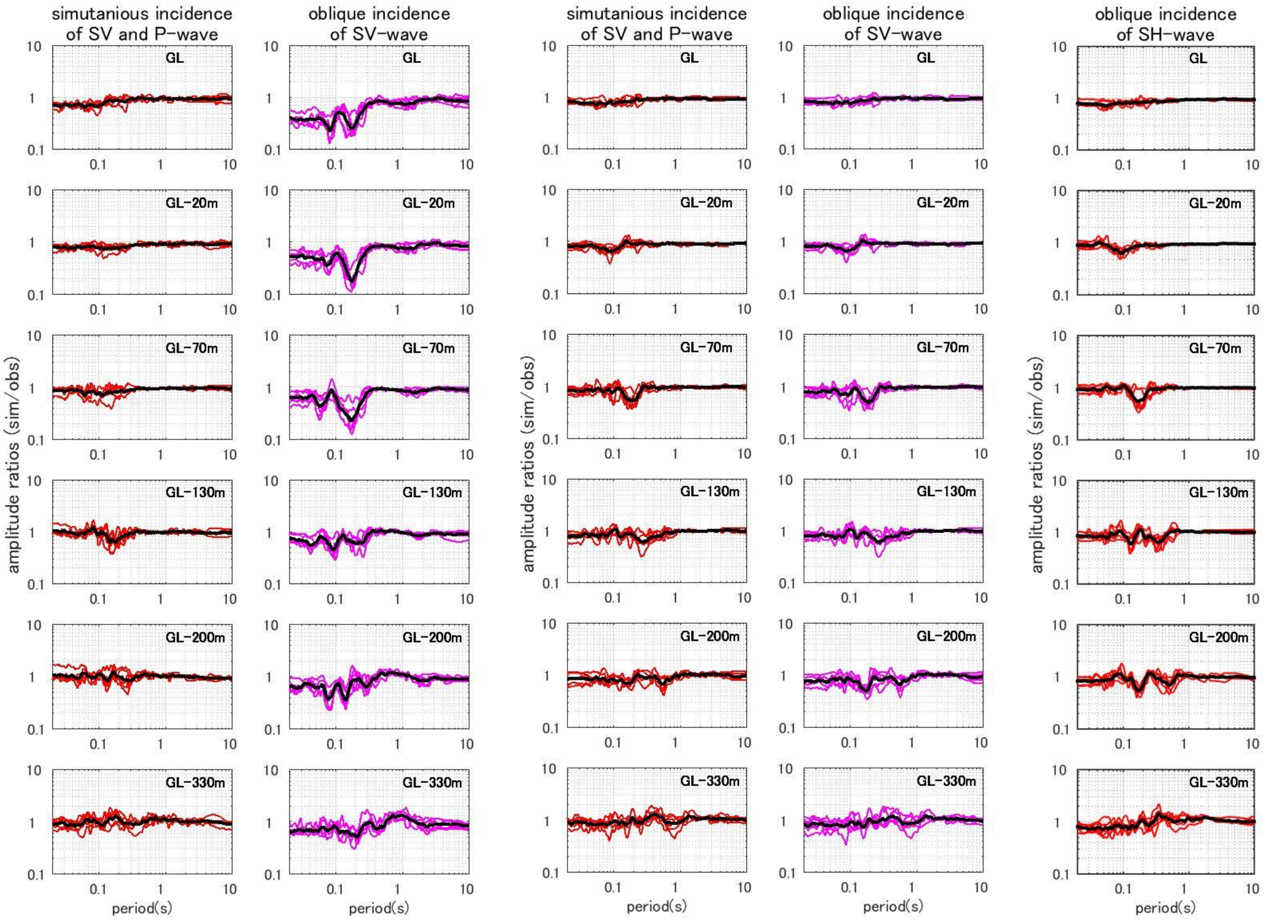

(a) vertical component

(b) horizontal radial component

(c) horizontal transverse component

Fig. 7 - Response spectra ratios of the simulations and the observed records (EQ01~EQ06).

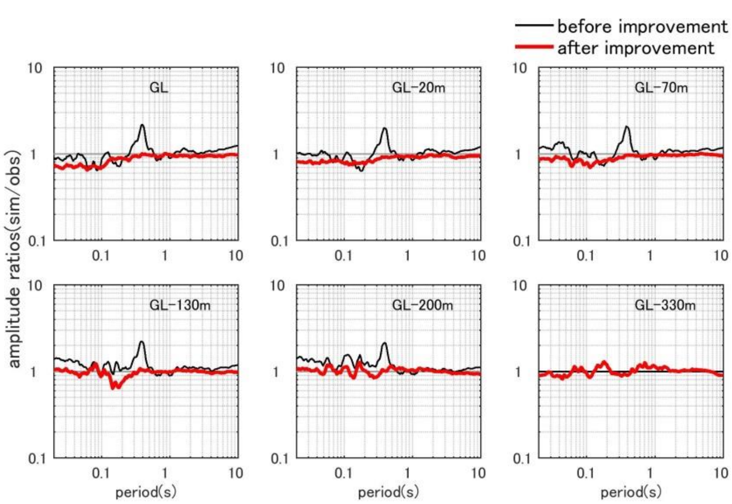

Fig. 8 - The comparison of simulations from before and after the improvement. Each line shows the average value of the response spectrum ratios of the simulated waves to the observed records for the vertical component of six earthquakes (EQ01~EQ06).

Thus, it is confirmed that the current method of estimating the incident wave by using all of the records of the vertical array better predicts the observed records than the conventional method using the bottom observation record.

4. Estimated incident wave

Here, we consider the incident wave estimated by this method. Fig. 9 shows the incident waves (P-wave, SV-wave, SH-wave) in the S-wave, which are estimated from all six earthquake records. Focusing on the magnitude relation of the incident wave amplitude for each earthquake, we can see that the amplitude of the P incident wave is too large to be ignored. For example, in EQ06, the maximum amplitude of the P incident wave of the S-wave is approximately 0.8 times the maximum amplitude of SV incident wave.

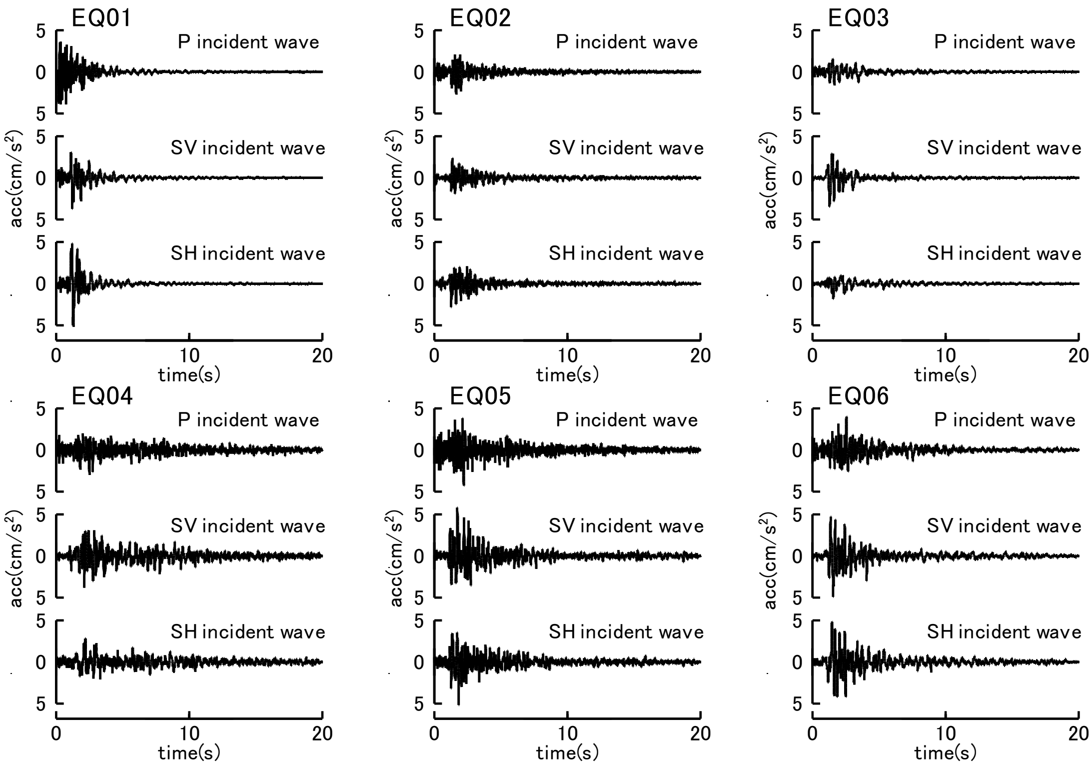

Fig. 9 – Estimated incident waves in the seismic basement.

In order to examine the proportion of the P incident wave in the S-wave, we examine the Fourier amplitude ratio of the SV and P incident waves, as shown in Fig. 10. Focusing on the average value of the six earthquakes, the ratios of P incident waves to SV incident waves are distributed between 0.4 and 2 times.

Hence, we determined that the recorded S-waves contain many components derived from P-incident waves.

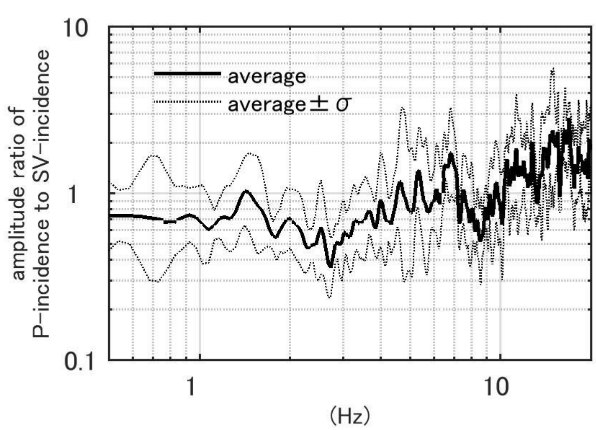

Fig. 10 - Fourier amplitude ratio of the estimated incident wave (S-waves).

5. Conclusions

In this study, we examined the evaluation method of horizontal and vertical 3-component motions in sedimentary layers. The following results were obtained:

(1) Regarding the method of Kyuke et al. (2010), which is used to evaluate vertical and horizontal radial motion in S-waves part, we pointed out that when we estimate the incident wave in bedrock using the records from the deepest sensor of the vertical array, the error in the ground model might be reflected strongly in the incident wave. This reduces the prediction accuracy. Then, we proposed a novel method that estimates the incident wave by using all of the records of the vertical array. Simultaneously, we expanded this method to SH incident waves in order to apply 3-component ground motions.

(2) By using the proposed method, we simulated the 3-component records at the IWK observation point, which has six vertical array observation points at various depths, down to the seismic basement. The simulation results of the 3-component waveforms, transfer functions, and response spectra are consistent with the observed records for each component. In addition, the vertical and horizontal radial components were compared with those of the conventional method, which assumes the oblique incidence of SV-waves. For the vertical component, the simulation results of our proposed method correlated well with the observed records compared with the results of the oblique incidence of the SV-wave. For the horizontal radial component, our proposed method and the method of oblique incidence of the SV-wave predict the observation records to the same degree.

(3) In order to confirm the effect of the new method that estimates incident waves using all of the records of vertical array, we compared the simulation results of this method to the previous one. For all three components, the simulated results obtained by this method show better correlation with the observed records compared with the before-improvement results.

(4) Furthermore, we examined the amount of P-incident wave in the S-wave, which was estimated by this method. The Fourier amplitude ratio of the P to the SV incident wave, estimated from the six earthquake records, showed that the ratio of P incident waves to SV incident waves are distributed between 0.4 and 2 times. Hence, we determined that the recorded S-waves contain many components derived from the P-incident wave.

6. Acknowledgement

In this study, we used the strong motion records that were provided by twelve Japanese Power Companies. We would like to thank all concerned.

7. References

[1] Takahashi, K., S. Ohno, M. Takemura, T. Ohta, T. Hatori, Y. Sugawara, and S. Omote (1992): Observation of earthquake strong - motion with deep borehole. Generation of vertical motion propagation in surface layers after S wave arrival, in Proc.*10th World Conference on Earthquake Engineering*, Spain., pp.1245-1250

[2] Tohdo, M., Hatori, T., CHiba, O., Takahashi, K., and Takemura, M. (1995): Characteristics of Vertical Seismic Motions and Qp-Values in Sedimentary Layers. *J. Struct. Constr. Eng., AIJ*, No. 475, pp.45-54

[3] Miake, M., Kusakabe, K., Maeda, Y., and Horike, M. (1999): A study on vertical component of synthesized waves using stochastic Green's function method, *Summaries of technical papers of annual meeting, AIJ*, B-2, pp.127-128

[4] Kyuke H, Sato Y, Kobayashi K, Tokumitsu R (2010): Study on a Method for Evaluating Vertical Seismic Ground Motion. *the 13th Japan Earthquake Engineering Symposium*, Japan., pp. 2313-2320

[5] The 12 Japanese Power Companies:Vertical seismic array network over Fukushima and Kanto region, CD-ROM, Japan Association for Earthquake Engineering